Electrostatic Surface Charge at Aqueous/α-Al$_2$O$_3$ Single-Crystal Interfaces as Probed by Optical Second-Harmonic Generation

Jeffrey P. Fitts,[†] Xiaoming Shang, George W. Flynn, Tony F. Heinz, and Kenneth B. Eisenthal*

Departments of Chemistry and Physics, Columbia University, New York, New York 10027

Received: April 19, 2004; In Final Form: November 26, 2004

Second harmonic generation (SHG) spectroscopy was used to characterize the pH-dependent electrostatic charging behavior of (0001) and (1$\bar{1}$02) crystallographic surfaces of corundum (α-Al$_2$O$_3$) single-crystal substrates. The pH value of the point of zero charge (pH$_{pzc}$) for each surface was determined by monitoring the SH response during three consecutive pH titrations conducted with 1, 10, and 100 mM NaNO$_3$ carbonate-free aqueous solutions. The crossing point of the three titration curves, which corresponds to the pH$_{pzc}$, occurs at pH 4.1 ± 0.4 for the (0001) surface and pH 5.2 ± 0.4 for the (1$\bar{1}$02) surface. SHG measurements that were recorded as a function of NaNO$_3$ concentration at fixed pH values were found to corroborate the pH$_{pzc}$ values identified in the pH titrations. A comparison of the SHG results with surface protonation constants calculated using a simple electrostatic model suggests that surface relaxation and bonding changes resulting from surface hydration do not account for differences between experimental observations and model predictions. The measured pH$_{pzc}$ values for the α-Al$_2$O$_3$ single-crystal surfaces are significantly more acidic than published values for Al–(hydr)oxide particles which typically range from pH 8 to 10. This discrepancy suggests that the charging behavior of Al–(hydr)oxide particles is determined by surface sites associated with defects assuming that differences in surface acidity reflect differences in the coordination environment and local structure of the potential-determining surface groups.

1. Introduction

Proton binding to oxide surfaces plays an important role in such diverse topics as nanoparticle phase stability,[1] ultrathin metal-film growth on metal oxides,[2] colloid aggregation,[3] sorption processes,[4] and soil chemistry.[5] Efforts to develop chemical models capable of predicting hydrated oxide surface properties in a wide range of natural and industrial systems require a fundamental understanding of the relationship between molecular-level surface structure and the protonation behavior of surface hydroxyl groups.[6–9] High quality single-crystal substrates and thin films serve as ideal model systems for fundamental studies of oxide surfaces because they are amenable to molecular-level probes and provide the means to use crystallographic orientation to control the variation of surface structure and types of surface groups. This model-system approach has been successfully used to investigate the crystallographic dependence of adsorbate geometries[10–12] and hydrated surface structures.[13,14] Here we investigate the structural dependence of surface acid/base properties by characterizing the pH-dependent charging behavior of two crystallographic surfaces of corundum (α-Al$_2$O$_3$) single-crystal substrates.

Second-harmonic generation (SHG) is uniquely suited for measuring generic surface charge properties of well-defined crystallographic surfaces. SHG, as a second-order nonlinear optical process is forbidden in centrosymmetric media.[15,16] SHG from the interface formed between water and any centrosymmetric oxide mineral is therefore sensitive to the structure and electronic properties of water molecules and oxide surface atoms in the narrow interfacial region where the inversion center is broken. In particular, SHG can be used to examine the charge state of the surface through the influence that the associated electric field has on the nonlinear response of the aligned water molecules.[17,18] Previous studies of both oxide particles and single-crystal substrates have demonstrated how SHG recorded as a function of bulk solution pH and ionic composition can be used to determine surface charge properties, including acid/base equilibrium constants and the pH value at which a surface has a net neutral charge (i.e., pH of the point of zero charge or pH$_{pzc}$).[17–20]

Published charge properties of Al–(hydr)oxide particles, which are commonly measured with potentiometry and electrophoresis methods, show significant variation. For example, pH$_{pzc}$ values reported for compositionally pure Al–(hydr)oxide particles that have been properly equilibrated in low-carbonate solutions range between pH 8 and 10.[21–23] Although this variation is typically attributed to sample history and environment, progress toward modeling these observations in terms of surface structure is hindered by the lack of experimental observations of highly constrained model surfaces, such as single-crystal substrates. Recent streaming potential and atomic force microscopy studies reported significant differences between the charging behavior of Al–(hydr)oxide particles and single-crystal substrates with isoelectric points, which are nearly identical to pH$_{pzc}$ values at low concentrations of monovalent electrolytes, for single-crystal surfaces occurring between pH 4 and 6.[20,22] The large uncertainties associated with these methods however do not permit a comparison of the charging behavior of different crystallographic surfaces.[22]

* To whom correspondence should be addressed. E-mail: eisenth@chem.columbia.edu.

† Current address: Environmental Sciences Department, Brookhaven National Lab, Upton, NY 11973.
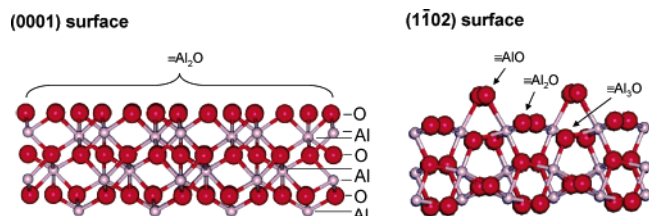
Figure 1. Side views of oxygen-terminated α-Al$_2$O$_3$ (0001) and (1$\bar{1}$02) surfaces that are consistent with hydrated structures proposed based on X-ray reflectivity studies.[13,14] The (0001) surface is terminated by O atoms coordinated to two Al atoms (i.e., ≡Al$_2$O or doubly coordinated oxygen atoms), while the (1$\bar{1}$02) surface is terminated by equal numbers of singly (≡AlO), doubly (≡Al$_2$O) and triply (≡Al$_3$O) coordinated oxygen atoms. Hydrogen atoms are not shown.
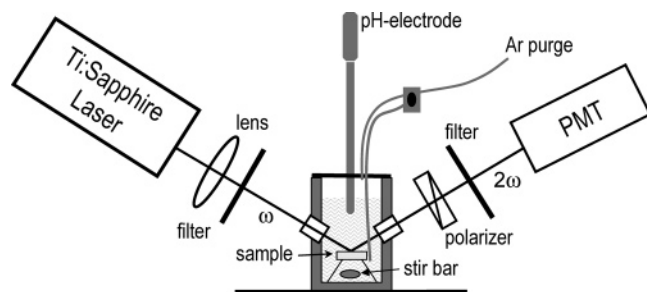
Figure 2. SHG experimental configuration and titration cell.

Here we use SHG to compare the charging behavior of the (0001) and (1$\bar{1}$02) crystallographic surfaces of α-Al$_2$O$_3$. These crystallographic surfaces are frequently used as model proxies for the basal and edge-type surfaces that are assumed to dominate Al−(hydr)oxide colloids and the aluminol (AlOH) layers in clay minerals.[10−12] The relevance of this model system is supported by an X-ray reflectivity study of a hydrated α-Al$_2$O$_3$ (0001) single-crystal surface that revealed a surface structure similar to the (0001) surface of the double-hydroxide layers that comprise the Al-hydroxide phases of gibbsite and bayerite.[13] A companion X-ray reflectivity study of the α-Al$_2$O$_3$ (1$\bar{1}$02) surface[14] highlighted the structural differences of the hydrated (0001) and (1$\bar{1}$02) surfaces. The hydrated surface structures proposed based on results from these published studies are compared in Figure 1. The structural distinctness of these two crystallographic surfaces are consistent with the experimentally observed differences in reactivity toward metal ions,[10−12] and water.[24,25] It has been assumed that the structural differences responsible for their disparate reactivity will also translate into significantly different acid/base characteristics and as a result different pH-dependent charging behaviors.[26] In the current study we measured the pH$_{pzc}$ values of the (0001) and (1$\bar{1}$02) single-crystal surfaces of α-Al$_2$O$_3$ in order to test this assumption. The results provide a basis for testing electrostatic model predictions and assessing the relative contribution by a clearly defined set of regular surface groups to the charging behavior of Al−(hydr)oxide particles.

2. Experimental Section

2.1. SHG Experimental Setup. The experimental configuration of the second harmonic measurements is shown in Figure 2. The laser source for the measurements was a modelocked Ti:sapphire laser (KMlab) which provided 0.66 W of 35 fs pulses at wavelength of 800 nm (corresponding to the fundamental angular frequency ω) at a repetition rate of 80 MHz. A pair of extra-cavity prisms was used to compensate for dispersion due to the sample measurement optics (including focusing lens and quartz window of the sample cell) and water that the

input beam passed through before reaching the sample surface. The dispersion compensation was optimized by moving the positions of the glass prisms to maximize the SH signal. To avoid thermal effects and sample damage, the input power was attenuated by a factor of 2 using an optical chopper with a duty cycle of 1:1. The p-polarized incident beam was focused onto the aqueous/α-Al$_2$O$_3$ interface with an estimated beam spot size diameter of ∼30 μm. The Teflon titration cell was designed for SHG measurements in the reflection geometry in order to accommodate centro-symmetric oxides that are not available as high-quality optically transparent prisms. The water-level in the cell was maintained above the quartz windows to avoid signal instabilities caused by water-level changes and disturbances. It should be noted that SHG from the water/quartz interface of the cell window can be ignored both because the incident beam was perpendicular to the window and the focal point of the input beam on the α-Al$_2$O$_3$ single-crystal was approximately 5 cm from the window. The second harmonic photons at a wavelength of 400 nm (corresponding to the SH angular frequency of 2ω) were separated from fundamental and background light with an interference filter prior to collection by a single-photon counting system. Only the p-polarized component of the SH was detected. Each data point in the figures below corresponds to the mean of three consecutive 100 s measurements.

2.2. Materials Preparation and Handling. Highly polished (1$\bar{1}$02) and (0001) α−Al$_2$O$_3$ single-crystal wafers were obtained from Bicron Industries. AFM images collected with a Nanoscope III Multimode scanning probe microscope from Digital Instruments show featureless single-crystal surfaces. These results are consistent with the 1−4 Å RMS roughness observed in previous X-ray reflectivity studies of single crystals prepared by the same methods.[27] X-ray photoelectron spectroscopy (XPS) survey scans reveal significant carbon contamination on the as-delivered crystals. Prior to each set of measurements the single-crystal surface was prepared with a 30 min acid etch in 10$^{−3}$ M HNO$_3$ followed by 30 min in a 300 °C N$_2$-purged tube furnace. The acid etching and baking steps were followed by multiple rinses with doubly distilled water, and removal of any remaining droplets with a high pressure argon stream. XPS survey scans indicate that carbon contamination is greatly reduced following this preparation procedure. Although exposure to air during sample transfer and laser alignment was unavoidable, great care was taken to ensure that the crystal was only exposed to argon-purged solutions throughout the experiment.

Only ultrahigh purity argon and nitrogen (99.999%) were used as purge gases. Sodium nitrate (Aldrich − 99.99%) was used as the electrolyte, and ACS reagent grade nitric acid (Aldrich) and low-carbonate sodium hydroxide (J. T. Baker Dilut-it) were used as titrants. Low-carbonate sodium hydroxide solutions were prepared in an argon-purged glovebag and sealed with rubber septa prior to each experiment. Sodium hydroxide additions were made using a syringe. Nitric acid and electrolyte stock solutions were purged prior to use.

2.3. pH Titrations. Immediately following the cleaning procedure described above the α-Al$_2$O$_3$ crystal was transferred to the Teflon titration cell, aligned in the laser beam and fixed to the base of the cell with Teflon clamps and screws. A Plexiglas cover was bolted in place to stabilize the titration cell and seal the cell environment to allow for an overpressure of argon. Once thoroughly purged with argon, the cell was filled with a 1 mM NaNO$_3$ solution. The solution pH was continuously monitored with a low-flow double junction glass electrode (Corning). After each pH adjustment (less than half of a pH

Aqueous/α-Al₂O₃ Single-Crystal Interfaces

J. Phys. Chem. B, Vol. 109, No. 16, 2005 **7983**
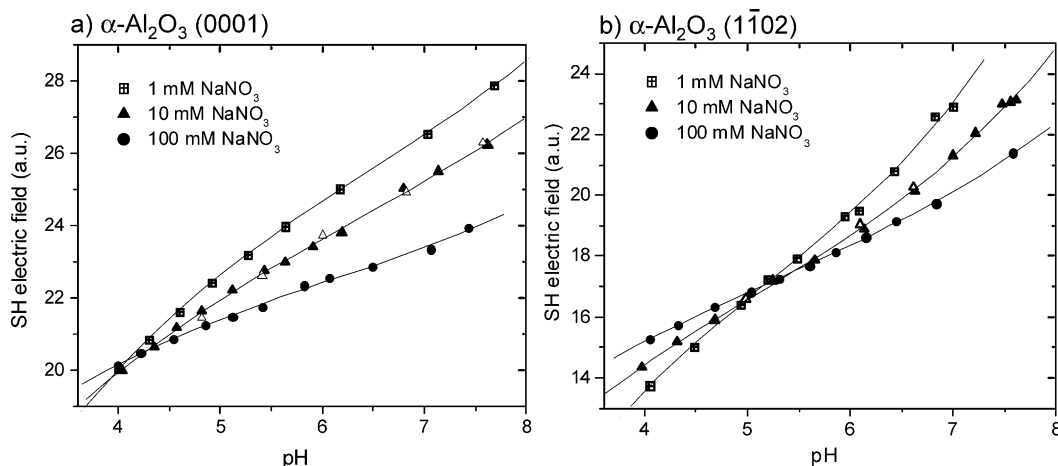
Figure 3. SH electric field from the water/α-Al₂O₃ (0001) and (1$\bar{1}$02) interfaces as the bulk solution pH is stepped between 7.5 and 4 at 1, 10, and 100 mM NaNO₃ concentrations. A base titration at 10 mM NaNO₃ is included in Figure 3a to demonstrate reversibility (open triangles) and a second 10 mM NaNO₃ acid titration is included in Figure 3b to demonstrate reproducibility (open triangles). Third-order polynomial fits are included to guide the eye.

unit) made during a titration, a 5 min equilibration period during which argon was bubbled through the solution was required for the SHG signal level to stabilize. Scattering by argon bubbles required that the bubbling be turned off during data collection, but otherwise a constant flow of argon in the titration cell headspace was maintained throughout the experiment. We determined that the purging procedures successfully prevented carbonate contamination by confirming that each pH step resulting from an acid or base addition was not buffered by carbonate. By comparison, in the absence of Ar-purging carbonate buffering was clearly observed.

Reversibility of the pH-dependent processes responsible for the observed change in the SHG response was indicated by consecutive acid and base titrations that showed no significant hysteresis. Process reversibility (i.e., reversibility of protonation and deprotonation of surface groups) indicates that a state of quasi-equilibrium was reached within 5 min following each acid/base addition. After completing 1, 10, and 100 mM NaNO₃ titrations, the cell solution was replaced with a fresh electrolyte solution and a titration at one of the electrolyte concentrations was repeated in order to check for both reproducibility and SH signal-level shifts caused by changes in alignment or laser power output.

3. Results

The variation in second-harmonic (SH) electric field strength (i.e., the square root of the measured intensity) as a function of bulk solution pH and electrolyte concentration is shown in Figure 3 for α-Al₂O₃ (0001) and (1$\bar{1}$02) single-crystal surfaces. The three titration curves cross at pH 4.1 ± 0.4 for the (0001) surface and pH 5.2 ± 0.4 for the (1$\bar{1}$02) surface. The relative uncertainty of the observed crossing point for an individual set of titration curves is quite low for single-crystal substrates from the same batch of crystals that had similar environmental histories. The observed crossing point, however, will likely vary depending on the source of the crystals, the surface preparation and the titration environment.

The results from this study are generally consistent with the crossover observed between pH 4 and 6 by Stack et al. for the (0001) surface of a corundum prism.[20] They referred to this crossover point as the point of zero salt effect (pzse). The SH electric field strength generated at a charged interface will depend on the bulk electrolyte concentration through the ionic screening of charged surface groups. The extent of ionic

screening affects the degree of alignment of the water dipoles in the static electric field of the charged surface, as well as the strength of the direct third-order nonlinear optical response to the presence of a dc field. The SH field strength, therefore, will be independent of the electrolyte concentration only at pH values where the surface has a net neutral charge. This will become apparent in the description of the model relating the SH electric field to the surface potential given below. With respect to the connection between the pH$_{pzc}$ and the pzse we note that in the absence of sorption reactions involving potential determining ions other than H⁺/OH⁻, the pzse is equivalent to the pH$_{pzc}$.[28]
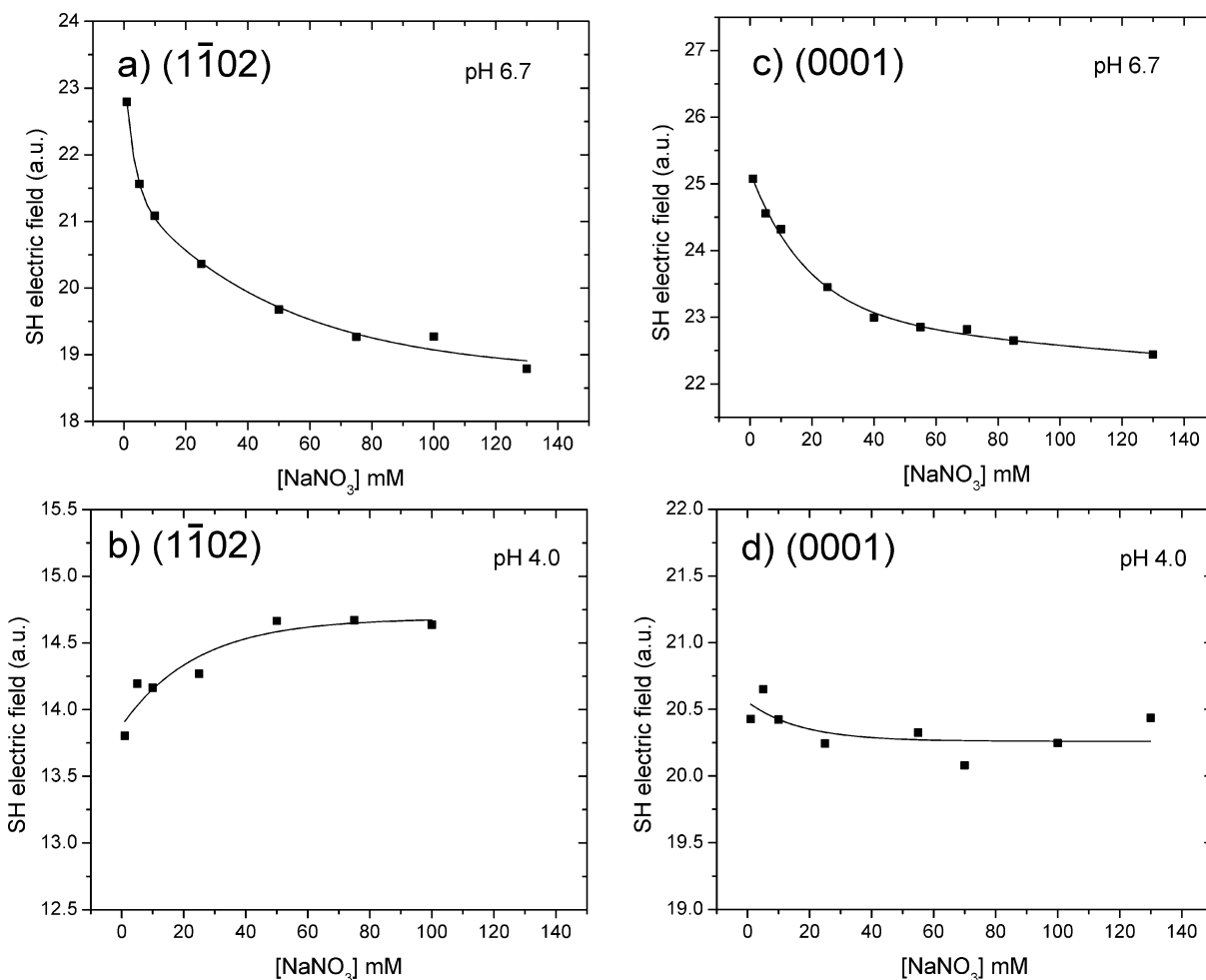
The electrolyte concentration dependence of the SH field strength observed at pH values above and below the pH$_{pzc}$ indicates that the α-Al₂O₃ (0001) and (1$\bar{1}$02) surfaces have a net charge. To explain how the observed electrolyte dependence reversal is related to the α-Al₂O₃ surface potential it is useful to consider a simple model for the interface nonlinear polarization of a charged surface $P_S^{(2)}$:

$$P_S^{(2)} = \chi_S^{(2)} E_\omega E_\omega + \chi_i^{(3)} E_\omega E_\omega E_{dc} \tag{1}$$

where E_ω is the incident field at frequency ω, $\chi_S^{(2)}$ is the second-order nonlinear response of the interface and $\chi_i^{(3)}$ is the third-order response of the water surrounding the interface. Since the region over which the dc-field is present because of charge screening, the bulk third-order response can be treated as part of the polarization sheet at the interface. The strength of this contribution is then proportional to $\int_\infty^0 \vec{E}_{dc}\, dz = \hat{z}.\ \int_\infty^0 E_{dc}\, dz = \Phi(0)$, i.e., to the surface potential at the interface which depends on electrolyte concentration and surface charge density.[18] Since the radiated SH field $E_{2\omega}$ is proportional to the interfacial nonlinear polarization $P_{2\omega}^{(2)}$, we can write for a fixed pump electric field E_ω:[18]

$$E_{2\omega} = A + B\Phi(0) \tag{2}$$

Here A corresponds to the nonlinear response from the system that is independent of the dc-electric field at the interface and represents SH light generated by chemical species at the α-Al₂O₃−water interface; B is a constant that is intrinsic to the field induced SH contribution from the charged interfaces. This model separates the SH field generated at the interface into a part independent of electrolyte concentration (A) and an electrolyte dependent part ($B\Phi(0)$). Applying this model we see

Figure 4. SH electric field from the water/α-Al$_2$O$_3$ (0001) and (1$\bar{1}$02) interfaces at pH 4.0 and 6.7 as a function of increasing electrolyte concentration. Lines are included to guide the eye.

that the reversal in electrolyte dependence of the SH field, i.e., an increase or decrease in the SH field as the electrolyte concentration increases for a given pH, indicates that the sign of the surface potential has changed.

In Figure 3b for the (1$\bar{1}$02) surface, the SH field strength decreases with increasing electrolyte concentration at pH values above 5.2. This dependence is reversed below pH 5.2. Additional SHG measurements recorded as a function of electrolyte concentration while the pH was fixed at 4 and 6.7 are shown in Figure 4 for the (0001) and (1$\bar{1}$02) surfaces. These measurements confirm the qualitative relationships between the SH field as a function of pH and electrolyte concentration observed in the pH-titration experiments at various fixed electrolyte concentrations (Figure 3). Furthermore, the magnitude of the changes in the SH field recorded in Figure 4a$-$c are within 5% of the equivalent changes observed in the pH titration experiments, and the fact that the SH field in Figure 4d does not change with electrolyte concentration is consistent with a pH$_{pzc}$ of 4.1 $\pm$ 0.4 for the (0001) surface.

4. Discussion

4.1. Acid/Base Characteristics of α-Al$_2$O$_3$ (0001) and (1$\bar{1}$02) Single-Crystal Surfaces. The SHG results show that the (0001) and (1$\bar{1}$02) surfaces of α-Al$_2$O$_3$ single-crystal substrates exhibit different pH$_{pzc}$ values. This result is in agreement with the commonly accepted assumption that each crystallographic surface possesses a unique set of potential-

determining surface groups, and therefore, should exhibit different acid/base characteristics. Recently published synchrotron X-ray reflectivity studies indicate that different sets of surface groups do in fact terminate hydrated α-Al$_2$O$_3$ (0001) and (1$\bar{1}$02) single-crystal surfaces.[13,14] The best-fit model of the diffraction results for the hydrated (0001) surface is most consistent with a terminating oxygen layer in which each oxygen atom is bonded to two Al atoms (Figure 1a).[13] The coordination of oxygen atoms in the (0001) surface plane is consistent with the bulk structure while Al$-$O bond lengths in the surface layers do differ from bulk values. In contrast, the hydrated (1$\bar{1}$02) surface is a more complex oxygen terminated surface in which oxygen surface atoms are coordinated variably to one, two and three Al atoms (Figure 1b).[14] Moreover, the position and bonding of oxygen atoms at the (1$\bar{1}$02) surface differ from oxygen atoms in the bulk structure. The consequences of these bonding changes in terms of the surface chemistry are discussed below.

Although the position of protons on single-crystal surfaces cannot be measured directly, synchrotron XPS studies show that both surfaces readily hydrolyze under moderate pressures of water vapor, and therefore, indicate that protonation reactions occur at regular surface sites on these two single-crystal surfaces.[24] By considering the ideal case of surfaces free from defects and contamination Trainer et al.[29] proposed that only $\equiv$Al$_2$O surface groups terminate the (0001) surface and equal numbers of $\equiv$AlO, $\equiv$Al$_2$O and $\equiv$Al$_3$O surface groups terminate

Aqueous/α-Al$_2$O$_3$ Single-Crystal Interfaces

J. Phys. Chem. B, Vol. 109, No. 16, 2005 **7985**

the (1$\bar{1}$02) surface. The acid/base equilibria and resulting charge at these surface groups can be written as follows,

$$\equiv AlOH^{0.5-} + H^+ \leftrightarrow \equiv AlOH_2^{0.5+} \quad \log(K) = 9.9 \quad (3)$$

$$\equiv Al_2O^- + H^+ \leftrightarrow \equiv Al_2OH^0 \quad \log(K) = 11.9 \quad (4)$$

$$\equiv Al_2OH^0 + H^+ \leftrightarrow \equiv Al_2OH_2^+ \quad \log(K) = 0 \quad (5)$$

$$\equiv Al_3O^{0.5-} + H^+ \leftrightarrow \equiv Al_3OH^{0.5+} \quad \log(K) = 5.9 \quad (6)$$

where $\equiv$ denotes a structural Al atom that completes its 6-fold coordination with at least one oxygen atom located in the terminating surface layer. A simple bond valence analysis was used to assign formal charges to the surface groups. Each 6-fold coordinated Al^{3+} contributes +0.5 v.u. (valence unit) and each direct H$^+$ bond contributes +1.0 v.u. to the saturation of the -2.0 v.u. net oxygen charge. The log(K) values are calculated with the multisite complexation (MUSIC) model which is based on a simple empirical model using Pauling's bond valence principles to estimate proton affinities of surface groups.[30] Two additional protonation states (i.e., $\equiv AlO^{1.5-}$ and $\equiv Al_3OH_2^{1.5+}$) are omitted from consideration since they are insignificant between pH 2 and 10. The calculated log(K) values do not consider structural relaxations resulting from changes in coordination of the surface oxygen atoms relative to the bulk structure.

On the basis of the model-derived log(K) values for $\equiv Al_2O$ surface groups, the p.z.c for the (0001) surface should occur at pH $\sim$ 6. The 12 log unit separation of the two log(K) values for reactions 4 and 5 indicates that the neutral surface species ($\equiv Al_2OH$) should predominate between pH 2 and 10. Therefore, this model predicts that a (0001) surface should not develop significant charge throughout the pH range of our titration. The SHG results clearly show pH-dependent charge development at the (0001) surface. Assuming that this model is correct, the experimentally observed surface charge must result from potential-determining surface groups not represented in reactions 3–6. Possible candidates including surface sites associated with defects or a surface contaminant are discussed below.

If the (1$\bar{1}$02) surface is terminated by an equal number of all three types of surface functional groups shown in reactions 3–6, as suggested by the X-ray reflectivity results for a hydrated (1$\bar{1}$02) surface, then the pH$_{pzc}$ should occur at pH $\sim$ 8. The charging behavior of this surface should be dominated by reactions 3 and 6 which predict significant charge development throughout the pH range of our titration. The model-predicted pzc value for the (1$\bar{1}$02) surface, however, is $\sim$2.8 pH units higher than the experimentally determined value of pH 5.2. Surface relaxations that result in contracted Al–O bonds within surface layers relative to bulk crystal bond lengths may account the discrepancy between model and experimental values. Fedkin et al.,[31] demonstrated how sensitive the MUSIC model is to bond length changes and how contracted bond lengths produce more acidic pH$_{pzc}$ values. The Al–O bond lengths at a hydrated surface that were determined by X-ray reflectivity for the surface groups shown in reaction 3 and 6, however, do not imply a significantly more acidic pH$_{pzc}$ value.[14]

4.2. Comparison with Al—(Hydr)oxide Particles. The pH$_{pzc}$ values observed in this study for α-Al$_2$O$_3$ single-crystal surfaces occur 3–6 pH units lower than the range of pH$_{pzc}$ values (pH 8–10) observed for compositionally pure Al—(hydr)oxide particles that have been equilibrated in low-carbonate aqueous solutions.[21,32,33] This difference in charging behavior is not consistent with the proposal that the charging behavior of Al—

(hydr)oxide particles can be modeled assuming that the reactive surface area is a combination of (0001) and (1$\bar{1}$02)-type surfaces.[26] This model, which assumes that the regular surface sites on (0001) and (1$\bar{1}$02) single-crystal surfaces also control the charging of Al—(hydr)oxide particles, requires that the pH$_{pzc}$ of one or both of the crystallographic surfaces occur between pH 8 and 10. Our results show that this is not the case, i.e., the pH$_{pzc}$ of the (0001) and (1$\bar{1}$02) faces are at pH 4.1 and 5.2, not between pH 8 and 10.

One possible explanation for the observed differences between the charging behavior of α-Al$_2$O$_3$ single-crystal substrates and Al—(hydr)oxide particles is that structurally unique regular surface sites, not present on the single-crystal surfaces, control the charging behavior of Al—(hydr)oxide particles. If we assume reactions (3–6) represent the complete set of potential-determining surface groups on both α-Al$_2$O$_3$ single crystals and Al—(hydr)oxide particles, then the observed differences in charging behavior (i.e., changes in acid/base equilibrium constants) must result from changes in local structures of the surface groups. Significant bond length variation of regular surface groups however is not consistent with the experimentally determined structures of hydrated α-Al$_2$O$_3$ single-crystal surfaces[13,14] nor with the surface structures of Al—(hydr)oxide particles inferred from known structures of layered Al—(hydr)-oxides, such as gibbsite and bayerite.[10,26]

Alternatively, the differences in experimentally determined charging properties may be attributed to a greater density of surface groups associated with defect sites on Al—(hydr)oxide particle surfaces. The featureless AFM images of the single-crystal surfaces used in the current study suggest a low step density and support the commonly accepted assumption that Al—(hydr)oxide particles have a greater density of steps and defects relative to single-crystal surfaces. The pH$_{pzc}$ values recorded for Al—(hydr)oxide particles can, therefore, result from protonation reactions occurring at surface groups associated with defects including steps, kinks, vacancies and domain boundaries. Although the atomic structures of surface groups associated with defects are not known, their presence will likely increase the density of surface oxygen atoms coordinated to a single structural Al atom (see reactions in eq 3). Given that reactions 4 and 5 do not contribute significant charge between pH 3 and 10, an increase in the surface density of reaction 3-type surface groups relative to reaction 6-type surface groups will result in a more basic pH$_{pzc}$ value. Therefore, more basic pH$_{pzc}$ values for Al—(hydr)oxide particles relative to single-crystal surfaces is consistent with higher defect densities for Al—(hydr)oxide particles.

While this qualitative model does predict that single-crystal surfaces with a low defect density will possess more acidic pH$_{pzc}$ values relative to particles, the protonation reactions occurring at regular surface groups on the terrace surface shown in reactions 3–6 cannot explain the SHG results. Surface contamination by carbonate and/or silicate species could be responsible for the measured pH$_{pzc}$ values of the single-crystal surfaces given that the specific adsorption of anions on metal-(hydr)oxide particles does produce more acidic pH$_{pzc}$ values.[34,35] For example, Su and Suarez recorded zeta potentials of carbonate-spiked colloid suspensions and observed that adsorbed carbonate species contribute negative charge to Al—(hydr)oxide particles at pH values as low as 4.[34] Every effort was made to exclude carbonate (Ar-purging) and silicate (solutions were never in contact with glass-ware) contamination from our experimental system. The absence of solution buffering and the fact that silicon was always below XPS detection limits suggest

that carbonate and silicate concentrations were effectively minimized. Surface contamination even at levels below solution buffering and XPS detection limits, however, may influence the pH$_{pzc}$ values of the single-crystal surfaces given that the low surface area-to-solution ratio and the relatively low density of sites associated with defects may make this experimental system sensitive to trace-levels of surface contamination. Whether surface contamination does play a role or not, the SHG results suggest that the types of surface groups that control the charging behavior of Al—(hydr)oxide particles, which are significant in soil chemistry, at most represent an insignificant portion of the charge-determining surface groups on the α-Al$_2$O$_3$ (0001) and (1$\bar{1}$02) single-crystal surfaces. We therefore conclude that the acid—base properties of Al—(hydr)oxide particles cannot be accounted for simply by a combination of the regular surface groups present on (0001) and (1$\bar{1}$02) surfaces, a result contrary to current models of particle charging behavior.

5. Conclusions

This work demonstrates the application of SHG measurements of planar single-crystal surfaces of centrosymmetric oxides to explore the relationship between generic charge properties and oxide surface structure. The results show that observed differences in the hydrated surface structures of α-Al$_2$O$_3$ (0001) and (1$\bar{1}$02) single-crystal substrates translate into differences in the surface acidity. The measured pH$_{pzc}$ values for the α-Al$_2$O$_3$ single-crystal surfaces (pH 4.1 and 5.2 for (0001) and (1$\bar{1}$02) surfaces, respectively) are significantly more acidic than published values for Al—(hydr)oxide particles which typically range from pH 8 to 10. We propose that the pH-dependent charging behavior of α-Al$_2$O$_3$ single-crystal surfaces and Al—(hydr)oxide particles likely reflect differences in coordination environment and local structure of the potential-determining surface groups. Our results raise the question as to whether recorded pH$_{pzc}$ values of single-crystal surfaces or particles reflect protonation reactions occurring at regular surface groups of the type shown in eqs 3−6 which are assumed to be common to both α-Al$_2$O$_3$ single-crystal and Al—(hydr)oxide particle surfaces. The results of this study suggest that surface sites associated with defects may determine the charge properties of Al—(hydr)oxide particles, and therefore, surface complexation models attempting to predict charging behavior based on surface structure must explicitly consider these types of sites.

References and Notes

(1) McHale, J. M.; Auroux, A.; Perrotta, A. J.; Navrotsky, A. *Science* **1997**, *277*, 788.

(2) Chambers, S. A.; Droubay, T.; Jennison, D. R.; Mattsson, T. R. *Science* **2002**, *297*, 827.

(3) Behrens, S. H.; Borkovec, M. *J. Phys. Chem. B* **1999**, *103*, 2918.

(4) Rietra, R.; Hiemstra, T.; van Riemsdijk, W. H. *Geochim. Cosmochim. Acta* **1999**, *63*, 3009.

(5) Sposito, G. *The Chemistry of Soils*; Oxford: New York, 1989.

(6) Rustad, J. R. Molecular models of surface relaxation, hydroxylation, and surface charging at oxide-water interfaces. In *Molecular Modeling Theory: Applications in the Geosciences*; 2001; Vol. 42, p 169.

(7) Sverjensky, D. A. *Geochim. Cosmochim. Acta* **2001**, *65*, 3643.

(8) Rustad, J. R.; Dixon, D. A.; Felmy, A. R. *Geochim. Cosmochim. Acta* **2000**, *64*, 1675.

(9) Hiemstra, T.; Vanriemsdijk, W. H.; Bolt, G. H. *J. Colloid Interface Sci.* **1989**, *133*, 91.

(10) Bargar, J. R.; Towle, S. N.; Brown, G. E.; Parks, G. A. *J. Colloid Interface Sci.* **1997**, *185*, 473.

(11) Trainor, T. P.; Fitts, J. P.; Templeton, A. S.; Grolimund, D.; Brown, G. E. *J. Colloid Interface Sci.* **2001**, *244*, 239.

(12) Templeton, A. S.; Trainor, T. P.; Traina, S. J.; Spormann, A. M.; Brown, G. E. *Proc. Natl. Acad. Sci. U.S.A.* **2001**, *98*, 11897.

(13) Eng, P. J.; Trainor, T. P.; Brown, G. E.; Waychunas, G. A.; Newville, M.; Sutton, S. R.; Rivers, M. L. *Science* **2000**, *288*, 1029.

(14) Trainor, T. P.; Eng, P. J.; Brown, G. E.; Robinson, I. K.; De Santis, M. *Surf. Sci.* **2002**, *496*, 238.

(15) Eisenthal, K. B. *Chem. Rev.* **1996**, *96*, 1343.

(16) Brevet, P.-F. *Surface second harmonic generation*, 1st ed.; Presses Polytechniques et Universitaires Romandes: Lausanne, Switzerland, 1997.

(17) Zhao, X. L.; Ong, S. W.; Eisenthal, K. B. *Chem. Phys. Lett.* **1993**, *202*, 513.

(18) Ong, S. W.; Zhao, X. L.; Eisenthal, K. B. *Chem. Phys. Lett.* **1992**, *191*, 327.

(19) Zhao, X. L.; Ong, S. W.; Wang, H. F.; Eisenthal, K. B. *Chem. Phys. Lett.* **1993**, *214*, 203.

(20) Stack, A. G.; Higgins, S. R.; Eggleston, C. M. *Geochim. Cosmochim. Acta* **2001**, *65*, 3055.

(21) Parks, G. A. *Chem. Rev.* **1965**, *65*, 177.

(22) Franks, G. V.; Meagher, L. *Colloids Surf. A* **2003**, *214*, 99.

(23) Kosmulski, M. *J. Colloid Interface Sci.* **2002**, *253*, 77.

(24) Liu, P.; Kendelewicz, T.; Brown, G. E.; Nelson, E. J.; Chambers, S. A. *Surf. Sci.* **1998**, *417*, 53.

(25) Schildbach, M. A.; Hamza, A. V. *Surf. Sci.* **1993**, *282*, 306.

(26) Hiemstra, T.; Yong, H.; Van Riemsdijk, W. H. *Langmuir* **1999**, *15*, 5942.

(27) Towle, S. N.; Bargar, J. R.; Brown, G. E.; Parks, G. A. *J. Colloid Interface Sci.* **1999**, *217*, 312.

(28) Sposito, G. *Environ. Sci. Technol.* **1998**, *32*, 2815.

(29) Trainor, T. P.; Templeton, A. S.; Brown, G. E.; Parks, G. A. *Langmuir* **2002**, *18*, 5782.

(30) Hiemstra, T.; Venema, P.; VanRiemsdijk, W. H. *J. Colloid Interface Sci.* **1996**, *184*, 680.

(31) Fedkin, M. V.; Zhou, X. Y. Y.; Kubicki, J. D.; Bandura, A. V.; Lvov, S. N.; Machesky, M. L.; Wesolowski, D. J. *Langmuir* **2003**, *19*, 3797.

(32) Hiemstra, T.; Vanriemsdijk, W. H.; Bruggenwert, M. G. M. *Neth. J. Agric. Sci.* **1987**, *35*, 281.

(33) Hayes, K. F.; Redden, G.; Ela, W.; Leckie, J. O. *J. Colloid Interface Sci.* **1991**, *142*, 448.

(34) Su, C. M.; Suarez, D. L. *Clay Clay Min.* **1997**, *45*, 814.

(35) Hingston, F. J.; Atkinson, R. J.; Posner, A. M.; Quirk, J. P. *Nature (London)* **1967**, *215*, 1459.